Supplementary Information

The Köppen-Geiger classification (Kottek et al. 2006) has been applied to the CMIP5 output. Figure S1 present the reference, mid-century and end-century periods for the RCP8.5 scenario. Overall the dominant climate type is arid (B), while to the south of the MENA equatorial (A) and to the north warm temperate (C) climates prevail. The spatial distribution of the climate types for the reference period agrees well with the observation-based results of Kottek et al (2006), except for fine scale details due to the coarse CMIP5 representation of orography. For example, the narrow region of the Fertile Crescent in the Levant is not well represented (for which we refer to MENA-CORDEX, see Zittis et al. 2014; Almazroui 2015).

The main climate classification is projected to remain similar in the mid-century period, for both scenarios. The most notable changes include the retreat of snow climates from elevated locations in favor of more temperate types, and the northward expansion of hot arid regimes in regions that were previously dominated by cold deserts and steppes. These climate shifts are more pronounced by the end of the century, especially according to the RCP8.5 scenario under which almost the entire MENA will become hot and arid, except the Anatolian peninsula and some hot arid summer-dry regions in Mesopotamia and northeastern Iran.

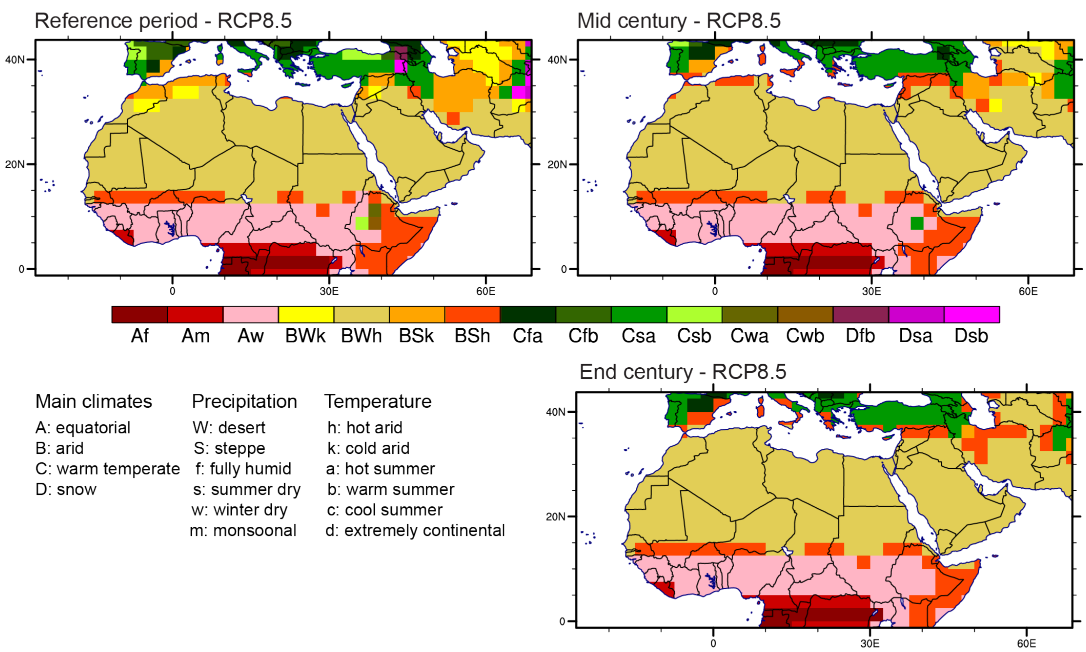

Fig. S1 Köppen-Geiger climate classification based on multi-model means for the reference period 1986–2005 (*top left*), the 2046–2065 (*top right*) and 2081–2000 (*bottom right*) periods according to the RCP8.5 scenario

Table S1 CMIP5 models from which simulation results are used in the present study

Modeling center	Institution	Model	Resolution (nx·ny·nz)
BCC	Beijing Climate Center, China Meteorological Administration	BCC-CSM1-1 BCC.CSM1-1(m)	128·64·L26 320·160·L26
CCCma	Canadian Center for Climate Modeling and Analysis	CanESM2	128·64·L35
CMCC	Centro Euro Mediterraneo per I Cambiamenti Climatici, Italy	CMCC-CM CMCC-CMS	480·240·L31 192·96·L95
CNRM-CERFACS	Centre National de Recherches Meteorologiques/Centre Europeen de Recherche et Formation Avances en Calcul Scientifique, France	CNRM-CM5	256·128·L31
SCIRO-BOM	Commonwealth Scientific and Industrial Research Organization, and Bureau of Meteorology, Australia	ACCESS1-0	192·145·L48
SCIRO-QCCCE	Commonwealth Scientific and Industrial Research Organization in Collaboration with the Queensland Climate Change Centre of Excellence, Australia	SCIRO-Mk3-6-0	192·96·L18
GCESS	College of Global Change and Earth System Science, Beijing Normal University	BNU-ESM	128·64·L26
INM	Institute for Numerical Mathematics, Russian Academy of Sciences	INM-CM4	180·120·L21
IPSL	Institut Pierre-Simon Laplace, France	IPSL-CM5A-LR IPSL-CM5B-LR	96·96·L39
LASG-CESS	LASG, Institute of Atmospheric Physics, Chinese Academy of Sciences, and CESS, Tsinghua University	FGOALS-g2	128·60·L26
LASG-IAP	LASG, Institute of Atmospheric Physics, Chinese Academy of Sciences	FGOALS-s2	128·108·L36
MIROC	Atmosphere and Ocean Research Institute (University of Tokyo), National Institute for Environmental Studies, and Japan Agency for Marine Earth Science and Technology	MIROC5	256·128·L40
MIROC	Japan Agency for Marine Earth Science and Technology, Atmosphere and Ocean Research Institute (University of Tokyo), and National Institute for Environmental Studies	MIROC-ESM MIROC-ESM-CHEM	128·64·L80
MOHC	Met Office Hadley Center, UK	HadGEM2-CC HadGEM2-ES	192·145·L40
MPI-M	Max Planck Institute for Meteorology, Germany	MPI-ESM-LR MPI-ESM-MR	192·96·L47 192·96·L95
MRI	Meteorological Research Institute, Japan	MPI-CGCM3	320·160·L48
NCAR	National Center for Atmospheric Research, USA	CCSM4	288·192·L26
NCC	Norwegian Climate Center	NorESM1-M	144·96·L26
NOAA-GFDL	National Oceanic and Atmospheric Administration, Geophysical Fluid Dynamics Laboratory, USA	GFDL-ESM2G GFDL-ESM2M	144·90·L24

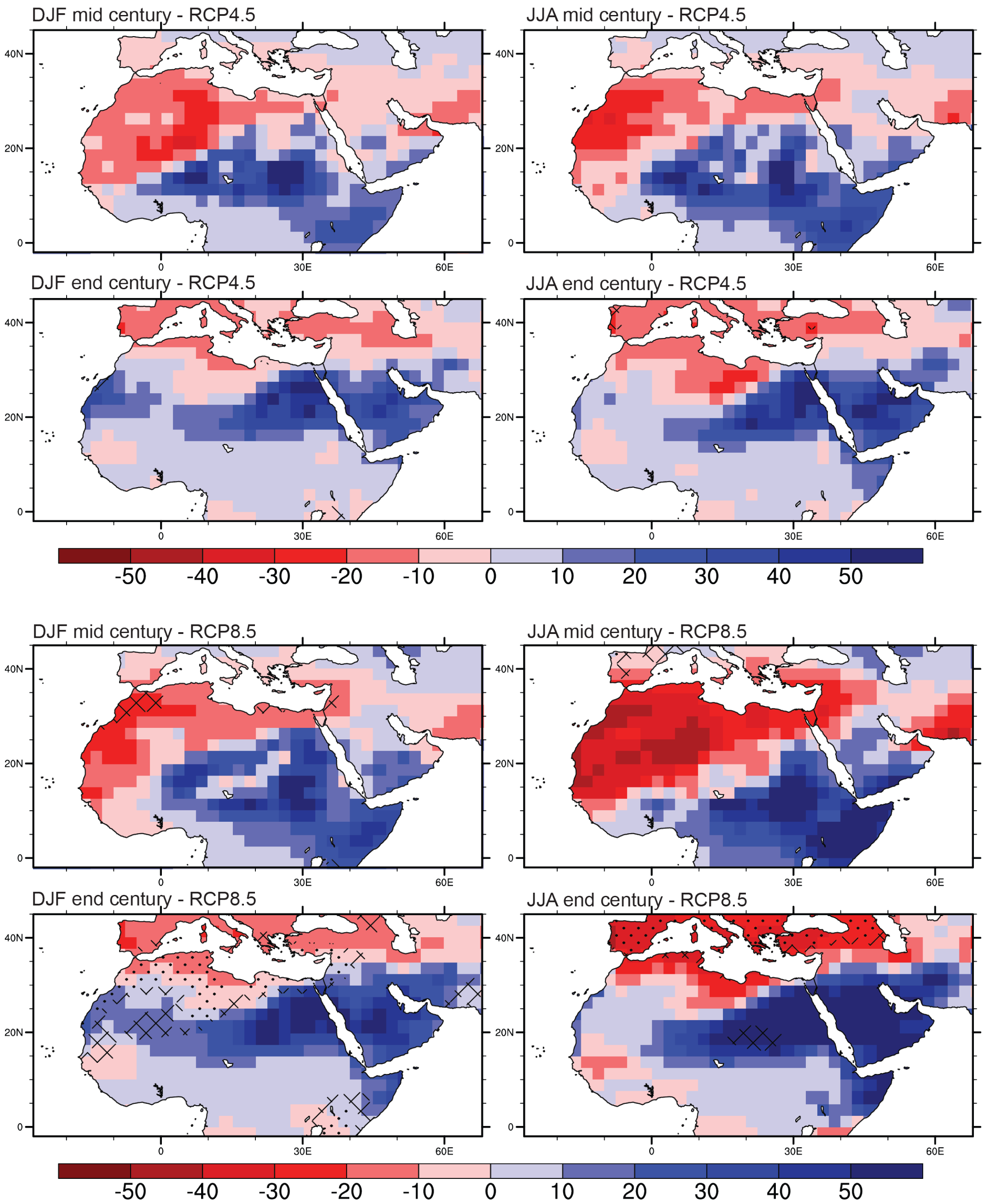

Fig. S2 Multi-model mean and robustness (dots $R \geq 0.5$, and cross-hatching $0.2 \leq R < 0.5$) for the fractional (%) precipitation (flux) change during DJF (*left*) and JJA (*right*) for 2046–2065 (mid-century) and 2081–2100 (end-century) relative to 1986–2005, according to the RCP4.5 and 8.5 scenarios. Notice that even though percentage precipitation increases might be large, the absolute amount can be small, especially in the MENA during summer. In view of the low robustness these results should be interpreted with caution

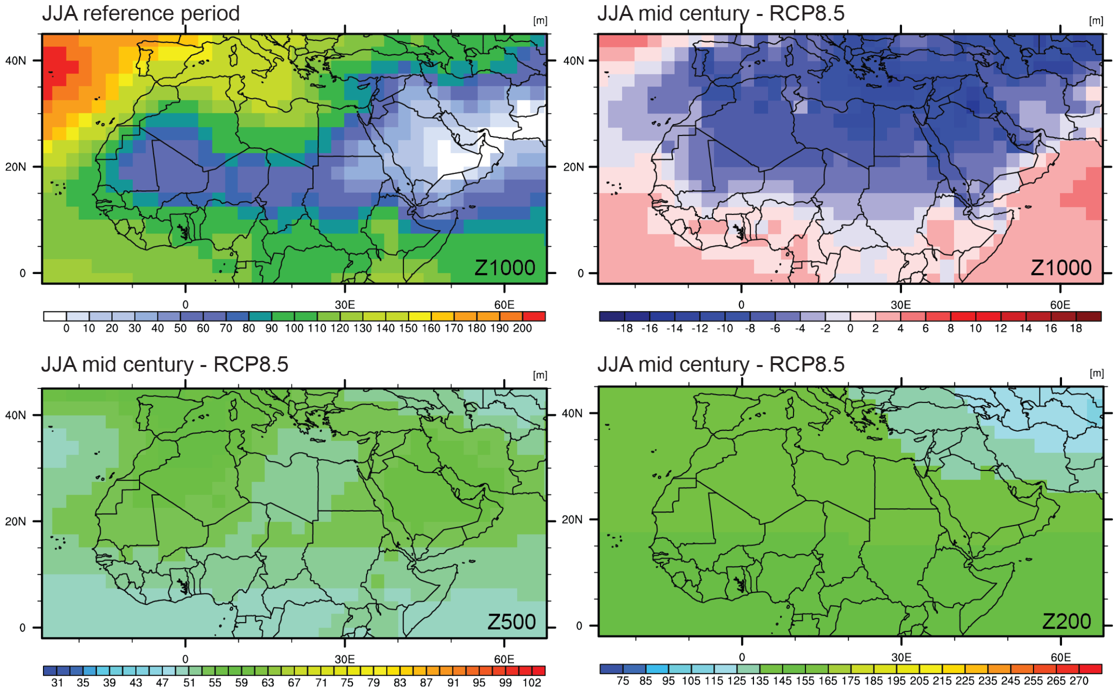

Fig. S3 Multi-model mean geopotential height levels (m) during summer at 1000 hPa in the reference period 1986–2005 (*upper left*) and changes from the reference period to 2046–2065 at 1000 hPa (*upper right*), 500 hPa (*lower left*) and 200 hPa (*lower right*) according to the RCP8.5 scenario

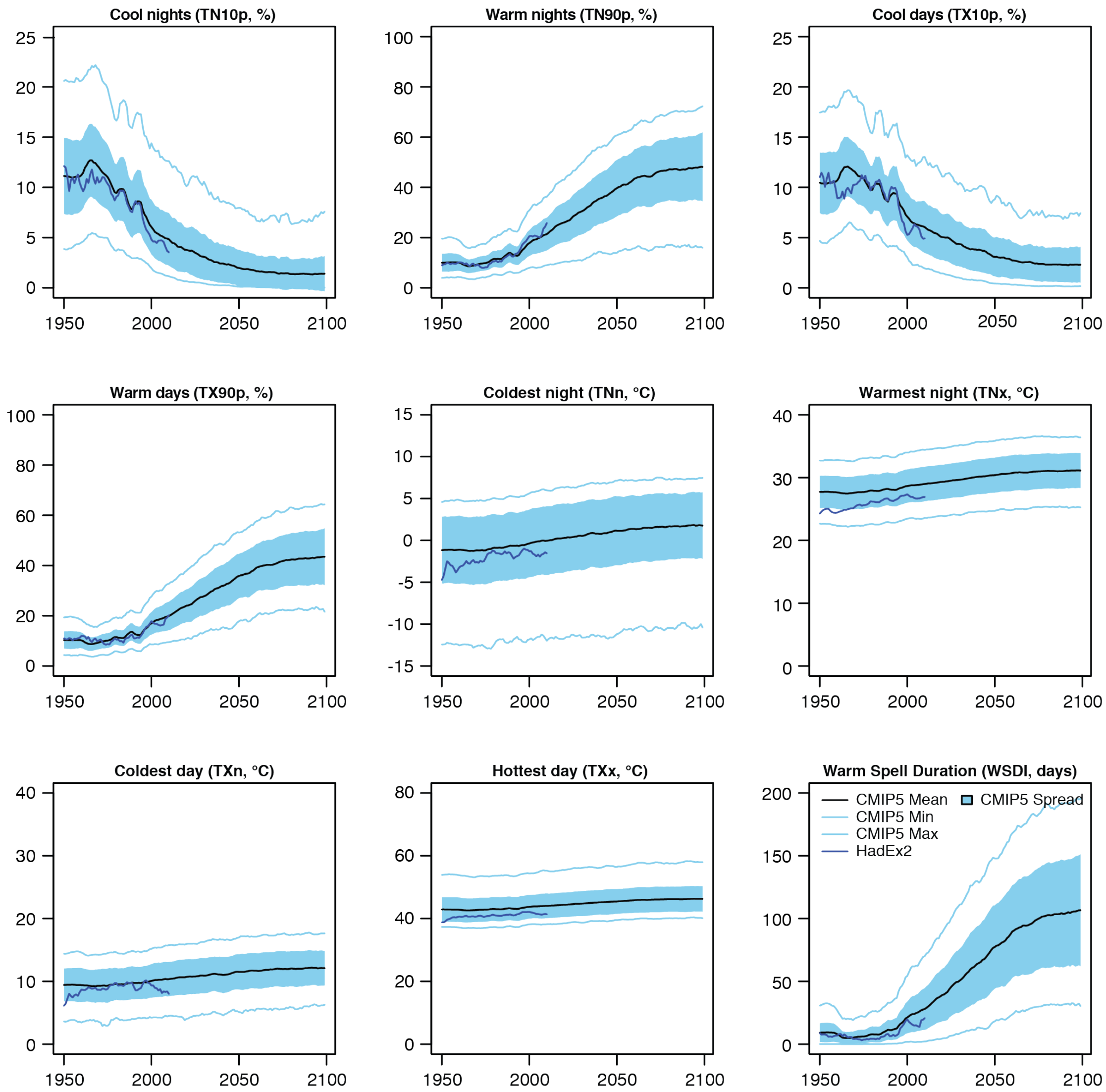

Fig. S4 Time evolution of temperature indices recommended by the ETCCDI calculated for the MENA from CMIP5 model results according to the RCP4.5 scenario, and from HadEX2 observations (dark blue lines)

References

Almazroui M (2015) RegCM4 in climate simulation over CORDEX-MENA/Arab domain: selection of suitable domain, convection and land-surface schemes. Int J Climatol, doi: 10.1002/joc.4340

Kottek M, Grieser J, Beck C, Rudolf B, Rubel F (2006) World map of the Köppen-Geiger climate classification updated. Meteorologische Zeitschrift 15: 259-263

Zittis G, Hadjinicolaou P, Lelieveld J (2014) CL-WRF sensitivity to physics parameterizations over the Middle East and North Africa. Am J Clim Change 3: 490-511